The Astronomical Journal, 131:1851–1863, 2006 March

NEAR-INFRARED COLOR PROPERTIES OF KUIPER BELT OBJECTS AND CENTAURS: FINAL RESULTS FROM THE ESO LARGE PROGRAM[1]

Audrey Delsanti[2]
Institute for Astronomy and NASA Astrobiology Institute, 2680 Woodlawn Drive, Honolulu, HI 96822; delsanti@ifa.hawaii.edu

Nuno Peixinho[2]
Centro de Astronomia e Astrofísica da Universidade de Lisboa, Observatorio Astronomico de Lisboa, Tapada da Ajuda, PT-1349-018 Lisbon, Portugal; peixinho@oal.ul.pt

Hermann Boehnhardt
Max Planck Institute for Solar System Research, Max-Planck-Strasse 2, D-37191 Katlenburg-Lindau, Germany; boehnhardt@linmpi.mpg.de

Antonella Barucci, Frédéric Merlin, and Alain Doressoundiram
LESIA, Observatoire de Paris-Meudon, 5 Place Jules Janssen, 92195 Meudon, France; antonella.barucci@obspm.fr, frederic.merlin@obspm.fr, alain.doressoundiram@obspm.fr

and

John K. Davies
Astronomy Technology Centre, Royal Observatory, Blackford Hill, Edinburgh EH9 3HJ, UK; jkd@roe.ac.uk
Received 2005 September 23; accepted 2005 October 25

ABSTRACT

We present near-IR *JHK* broadband photometry for 17 Kuiper Belt objects (KBOs) and Centaurs. The observations were performed within the ESO Large Program on the "Physical Properties of Kuiper Belt Objects and Centaurs" from 2001 January to 2002 August. We used the ISAAC instrument at the ESO 8 m Very Large Telescope. We compiled visible–near-IR colors for a total of 51 published objects and performed a statistical analysis. Color-color correlations show that the same coloring process is probably acting on Centaur and KBO surfaces in the visible–near-IR range. Centaurs with $H - K$ smaller than the Sun (0.06) systematically display the reddest $B - V$ colors (at the 2.5 σ level). These Centaur surfaces are suspected of harboring material that has spectral signatures around 1.7–2.2 μm (water ice is a possibility; it was reported for the three objects that have published spectroscopy). We report no statistically significant evidence for a bimodal structure of the *VJHK* Centaur colors (Kolmogorov-Smirnov and dip tests on up to 17 objects). The Centaur $H - K$ colors show some robust evidence (significance level >99.99%) for a continuous structure. We also report a statistically significant bimodal structure of the Centaur $B - R$ distribution, which is compatible with the results published by Peixinho et al. in 2003 with different data. Classical KBOs show no trends at the 3 σ level. The $V - J$ color is marginally correlated with perihelion distance q (which is consistent with results reported by Doressoundiram et al. in 2005 on $B - R$ colors). Resonant and scattered disk objects are underrepresented (seven and nine objects, respectively) and show no statistically significant trend. Some of the marginal trends are mentioned as worthy of subsequent monitoring.

Key words: infrared: solar system — Kuiper Belt — methods: statistical — techniques: photometric

Online material: color figures, machine-readable tables

1. INTRODUCTION

The region of the solar system beyond Neptune is populated by icy minor bodies known as trans-Neptunian objects or Kuiper Belt objects (KBOs). Since the discovery of 1992 QB_1 (Jewitt & Luu 1993), more than 1000 such objects have been detected. Due to their large heliocentric distances, KBOs are suspected of retaining the most pristine solar system material. From a dynamical point of view, KBOs are classified as classical objects (with circular orbits of moderate eccentricities), resonant objects, trapped in mean motion resonances with Neptune (the 3 : 2 resonance hosts the "Plutinos," named after the largest of them, Pluto), and scattered disk objects (SDOs). SDOs are believed to have had gravitational interactions with giant planets at some point in their history, which caused their orbits to become eccentric and sometimes very inclined. Two extreme objects have been classified as "extended scattered disk" objects (Gladman et al. 2002); their perihelia are far outside the orbit of Neptune. Due to their faintness, KBOs are very difficult to study; their physical properties are far from being fully studied and understood (see summary by Barucci et al. 2004). Basic parameters such as size and albedo are known for only a few objects and are difficult to measure.

Physical information about KBOs comes from surface color measurements made through broadband filters in the visible–near-IR range, but such photometry provides only a general insight into KBOs' physical properties. Surface composition is determined by reflectance spectroscopy. However, even with the use of 8–10 m class telescopes, only the brightest KBOs ($m_V \sim 17$–20) can be studied. For a review on the current state of knowledge of the Kuiper Belt, please refer to Barucci (2003), Davies & Barrera (2004), or Delsanti & Jewitt (2006).

The optical color diversity among the observed KBOs and Centaurs seems to extend to near-IR wavelengths, although

[1] Based on observations collected at the European Southern Observatory, Chile, under program 167.C-0340.

[2] LESIA, Observatoire de Paris-Meudon, 5 Place Jules Janssen, 92195 Meudon, France.

TABLE 1
Observational Circumstances

Object	Type	UT Date	r (AU)	Δ (AU)	α^o (deg)
1999 CD_{158}	Classical	2002 Jan 21	48.22	47.23	0.0
2000 OJ_{67}	Classical	2001 Nov 12	42.59	42.56	1.3
2000 PE_{30}	SDO	2001 Oct 11	37.09	36.79	1.5
2001 CZ_{31}	Classical	2001 Apr 14	41.39	41.07	1.3
2001 QF_{298}	3:2	2002 Aug 15	42.62	41.72	0.6
(10370) Hylonome	Centaur	2002 Feb 13	19.46	19.20	2.8
(15820) 1994 TB	3:2	2001 Aug 16	29.35	28.64	1.4
(26181) 1996 GQ_{21}	SDO	2001 May 9	39.28	38.32	0.4
(26375) 1999 DE_9	SDO	2001 May 9	34.00	33.79	1.6
(33128) 1998 BU_{48}	Centaur	2001 Apr 11	27.66	27.17	1.8
(33340) 1998 VG_{44}	3:2	2001 Sep 18	30.20	29.82	1.8
(40314) 1999 KR_{16}	SDO	2001 Apr 21	37.81	36.81	0.1
(44594) 1999 OX_3	Centaur	2002 Aug 15	26.29	25.31	0.5
(52872) Okyrhoe	Centaur	2002 Aug 16	8.76	8.60	6.5
(60558) 2000 EC_{98}	Centaur	2002 Jan 15	14.94	14.49	3.4
(66652) 1999 RZ_{253}	Classical	2002 Aug 16	41.02	40.01	0.2
(79360) 1997 CS_{29}	Classical	2001 Nov 19	43.58	43.14	1.2

Note.—SDO = scattered disk object, 3:2 = resonant object, α^o = phase angle at time of observation.

relatively few visible–near-IR color data sets are available (see Delsanti et al. 2004; McBride et al. 2003 and references therein). Statistical analyses point to correlations between optical colors and some orbital parameters (i, e, q) for the classical objects (e.g., Hainaut & Delsanti 2002; Trujillo & Brown 2002; Doressoundiram et al. 2002; Peixinho et al. 2004). In contrast, no similar trends are obvious for Plutinos, SDOs, or Centaurs. Another important result is the absence of any correlation of colors with size or heliocentric distance for any of these populations. Here we investigate whether similar trends exist for near-IR colors. Centaur visible colors display a bimodal structure that is statistically significant for the $B - R$ index (Peixinho et al. 2003). This bimodal structure is difficult to understand from a physical point of view, and to date, no model has succeeded in reproducing the observed Centaur color distributions. In this paper, we present *JHK* colors for 17 Centaurs and KBOs. We then merge this sample with existing data to analyze a data set of 51 objects with different statistical tools.

2. THE ESO LARGE PROGRAM

This program was designed in the early 2000s under the leadership of H. Boehnhardt. At that time, visible surface colors were known for only a few objects (see, for instance, Luu & Jewitt 1996; Green et al. 1997; Jewitt & Luu 1998; Barucci et al. 1999), and near-IR (mostly J) colors were known for an even smaller subset of KBOs (Green et al. 1997; Weintraub et al. 1997; Davies et al. 1998; McBride et al. 1999). A few spectra were published (Brown & Koresko 1998; Brown et al. 1999; Barucci et al. 1999a). The goal of the ESO Large Program was to provide observational constraints to characterize the physical properties of a relatively large number of KBOs and Centaurs, using the collecting power of the four 8 m Very Large Telescopes at Cerro Paranal Observatory, Chile. The program started in 2001 and encompassed photometric and spectroscopic measurements at visible and near-IR wavelengths for a total of 100 objects. The same instrumental setup was used during the whole program (~300 hr spread over 2 yr) to ensure a highly homogeneous data set. The results of this program are presented in Boehnhardt et al. (2002), Peixinho et al. (2004), and this paper for the photometry and Barucci et al. (2002), Dotto et al. (2003), Doressoundiram et al. (2003, 2006), Lazzarin et al. (2003), and Fornasier et al. (2004) for the spectroscopy.

3. OBSERVATIONS

The near-IR photometry observations were carried out at the ESO 8 m Very Large Telescope, Unit 1. We used the ISAAC (Infrared Spectrometer and Array Camera) instrument (installed at the Nasmyth B focus) in the short-wavelength (SW) imaging mode. The SW arm is equipped with a 1024×1024 Hawaii Rockwell array with 18.5×18.5 μm^2 pixels. The pixel scale is $0''.148$ pixel^{-1}, and the field of view is $2'.5 \times 2'.5$. We used the J, H, and K_s filters, which have central wavelengths of 1.25, 1.65, and 2.16 μm, respectively, and a width of ~0.3 μm.

The object list and the geometric circumstances of the observations are summarized in Table 1. Some of the observations were executed in service mode over a period from 2001 April to 2002 January, when the observational constraints (e.g., seeing better than $0''.8$ and photometric or clear weather) were fulfilled. Observations from 2002 August were carried out in visitor mode. In both cases, imaging was done using a standard jittering method, dithering the telescope within $10''$ between two subexposures according to a random pattern. The telescope was tracked at the sidereal rate since the KBO apparent velocities are below $4''$ hr^{-1} and the typical image seeing is $0''.65$. Thus, there is no trailing of the KBOs with respect to the stars on a single subexposure (less than a minute in all filters).

4. DATA REDUCTION AND PHOTOMETRY

We corrected all frames for the "electrical ghost" effect before dark subtraction. We then applied a flat-field correction. Sky correction was performed using IRAF *xdimsum*, a package optimized for background-dominated data. The complete method is described in Delsanti et al. (2004). We recombined the individual sky-subtracted frames following two methods. We first stacked the images using multiple star centroids to get pointlike stars. This composite was used for point-spread function estimation. In a second version, we took into account the KBO velocity (obtained from the JPL ephemeris) to stack the images. This composite (with a pointlike KBO) was used for KBO photometry measurements.

TABLE 2
PHOTOMETRIC MEASUREMENTS

Object	UT Date	Time[a]	Filter	Magnitude
1999 CD_{158}	2002 Jan 21	05:10	*H*	19.99 ± 0.07
	2002 Jan 21	05:57	*H*	20.05 ± 0.07
	2002 Jan 21	06:29	*J*	20.45 ± 0.06
	2002 Jan 21	06:47	*K*	19.94 ± 0.06
2000 OJ_{67}	2001 Nov 12	00:04	*H*	20.74 ± 0.07
	2001 Nov 12	01:02	*J*	21.01 ± 0.06
	2001 Nov 12	01:17	*K*	20.67 ± 0.12
	2001 Nov 12	01:57	*J*	21.04 ± 0.07
	2001 Nov 12	02:11	*K*	20.61 ± 0.12
2000 PE_{30}	2001 Oct 11	01:13	*H*	20.34 ± 0.04
	2001 Oct 11	02:11	*J*	20.78 ± 0.04
	2001 Oct 11	02:26	*K*	20.08 ± 0.06
	2001 Oct 11	03:06	*J*	20.75 ± 0.04
	2001 Oct 11	03:18	*K*	20.11 ± 0.06
2001 CZ_{31}	2001 Apr 14	00:15	*J*	20.82 ± 0.07
	2001 Apr 14	00:19	*H*	20.27 ± 0.07
	2001 Apr 14	00:32	*K*	20.11 ± 0.07
2001 QF_{298}	2002 Aug 15	03:10	*J*	20.27 ± 0.06
	2002 Aug 15	03:20	*H*	20.04 ± 0.06
	2002 Aug 15	03:40	*K*	19.84 ± 0.07
	2002 Aug 15	03:54	*J*	20.23 ± 0.05
	2002 Aug 15	09:30	*J*	20.21 ± 0.05
	2002 Aug 15	09:40	*H*	19.99 ± 0.08
	2002 Aug 15	10:00	*K*	19.87 ± 0.09
	2002 Aug 16	10:05	*J*	20.21 ± 0.05
(10370) Hylonome	2002 Feb 13	07:31	*H*	20.66 ± 0.06
	2002 Feb 13	07:59	*J*	20.84 ± 0.06
	2002 Feb 13	08:06	*K*	20.39 ± 0.07
	2002 Feb 13	09:01	*J*	20.95 ± 0.05
(15820) 1994 TB	2001 Aug 16	06:48	*J*	20.57 ± 0.06
	2001 Aug 16	07:06	*H*	20.19 ± 0.06
	2001 Aug 16	08:07	*J*	20.62 ± 0.08
(26181) 1996 GQ_{21}	2001 May 9	02:43	*J*	18.72 ± 0.07
	2001 May 9	02:48	*H*	18.24 ± 0.06
	2001 May 9	03:14	*J*	18.73 ± 0.07
	2001 May 9	03:19	*K*	18.19 ± 0.06
(26375) 1999 DE_9	2001 May 9	01:51	*J*	18.78 ± 0.08
	2001 May 9	01:54	*H*	18.46 ± 0.08
	2001 May 9	02:08	*K*	18.50 ± 0.08
(33128) 1998 BU_{48}	2001 Apr 11	23:45	*J*	19.86 ± 0.08
	2001 Apr 11	00:02	*H*	19.51 ± 0.06
	2001 Apr 11	00:59	*J*	20.03 ± 0.08
	2001 Apr 11	01:15	*K*	19.70 ± 0.07
(33340) 1998 VG_{44}	2001 Sep 18	07:24	*J*	20.03 ± 0.06
	2001 Sep 18	07:36	*H*	19.58 ± 0.05
	2001 Sep 18	08:28	*J*	19.99 ± 0.06
	2001 Sep 18	08:41	*K*	19.57 ± 0.06
(40314) 1999 KR_{16}	2001 Apr 21	04:08	*J*	19.56 ± 0.05
	2001 Apr 21	04:20	*H*	18.96 ± 0.05
	2001 Apr 21	05:04	*J*	19.52 ± 0.05
	2001 Apr 21	05:16	*K*	18.94 ± 0.05
(44594) 1999 OX_3	2002 Aug 15	00:00	*H*	19.19 ± 0.04
	2002 Aug 15	00:20	*K*	19.19 ± 0.07
	2002 Aug 15	00:35	*J*	19.63 ± 0.04
	2002 Aug 16	00:10	*H*	19.15 ± 0.06
	2002 Aug 16	00:30	*K*	19.20 ± 0.07
	2002 Aug 16	00:50	*J*	19.67 ± 0.04
(52872) Okyrhoe	2002 Aug 16	06:10	*J*	19.04 ± 0.03
	2002 Aug 16	06:20	*H*	18.54 ± 0.05
	2002 Aug 16	06:40	*K*	18.41 ± 0.05
	2002 Aug 16	07:00	*J*	19.09 ± 0.03
	2002 Aug 16	08:45	*J*	19.05 ± 0.03
	2002 Aug 16	08:55	*H*	18.68 ± 0.05
	2002 Aug 16	09:15	*K*	18.49 ± 0.06
	2002 Aug 16	09:30	*J*	19.13 ± 0.03
(60558) 2000 EC_{98}	2002 Jan 16	07:45	*H*	19.91 ± 0.05
	2002 Jan 16	08:14	*J*	20.48 ± 0.06
	2002 Jan 16	08:21	*K*	19.57 ± 0.04
	2002 Jan 16	09:20	*J*	20.45 ± 0.05
(66652) 1999 RZ_{253}	2002 Aug 16	07:10	*J*	20.08 ± 0.05
	2002 Aug 16	07:30	*H*	19.59 ± 0.08
	2002 Aug 16	08:00	*K*	19.49 ± 0.05
	2002 Aug 16	08:30	*J*	20.02 ± 0.05
(79360) 1997 CS_{29}	2001 Nov 19	07:23	*H*	19.74 ± 0.06
	2001 Nov 19	07:52	*J*	20.11 ± 0.06
	2001 Nov 19	07:58	*K*	19.70 ± 0.06
	2001 Nov 19	08:55	*J*	20.13 ± 0.06

NOTE.—Table 2 is also available in machine-readable form in the electronic edition of the *Astronomical Journal*.
[a] UT times are midexposure.

We used standard stars (Las Campanas Observatory/Palomar NICMOS catalog; Persson et al. 1998) to estimate the zero point of the instrument in the different filters. We used Paranal Observatory typical extinction values provided by the ESO calibration plan, which are $k_J = 0.11$, $k_H = 0.06$, and $k_K = 0.07$ mag per air mass. We neglected the instrument color transformations, as they lie below 1% for our solar system objects.

We used an aperture correction method to measure the KBOs' flux, as fully described in Delsanti et al. (2004). The sky background was estimated using five square apertures (of 25 pixels, i.e., 3″.7 in size) surrounding the object. We constructed a curve of growth for several nonsaturated nearby stars in order to compute the aperture correction. The KBO magnitudes obtained using this method are listed in Table 2. UT times are given at midexposures. The error estimation on magnitudes ranges from 3% to 12%, depending on the objects. The errors include error from the photometric calibration (systematic; a few percent), error on the flux measurement (around 1%–2%; contains the photon/instrumental noises), and error from the aperture correction (typically from 1%–2% up to 8% depending on the quality and number of nearby stars found to build the curves of growth).

Table 3 shows the solar colors and *JHK* colors for 17 objects from this paper (nine of them are published for the first time) and a summary of the ESO Large Program *JHK* photometry obtained within the spectroscopy part of the program. When multiple magnitudes of a given filter are available, color indexes are computed from the magnitudes closest in time.

5. RESULTS

5.1. *Dynamical Classification of the Objects*

There is currently no dynamical classification universally accepted by the community for the objects we are dealing with. The Minor Planet Center provides on a daily basis two different lists of orbital parameters: one for the trans-Neptunian objects and one for the Centaurs and scattered disk objects,[3] with no further

[3] See http://cfa-www.harvard.edu/iau/lists/TNOs.html and http://cfa-www.harvard.edu/iau/lists/Centaurs.html, respectively.

TABLE 3
ESO Large Program Near-IR Colors

Object	$J-H\pm\sigma$	$H-K\pm\sigma$	$J-K\pm\sigma$	Reference
Solar Colors and Objects from This Paper				
Solar colors	0.23	0.06	0.29	Hardorp (1980), Hartmann et al. (1982)
1999 CD_{158}	$0.43\pm0.09^{\dagger}$	$0.08\pm0.09^{\dagger}$	0.51 ± 0.08	This paper
2000 OJ_{67}	$0.28\pm0.09^{*}$	0.07 ± 0.12	$0.35\pm0.12^{*}$	This paper
2000 PE_{30}	$0.42\pm0.05^{*}$	$0.25\pm0.07^{\ddagger}$	$0.67\pm0.07^{*,\ddagger}$	This paper
2001 CZ_{31}	0.55 ± 0.09	0.16 ± 0.09	0.71 ± 0.09	This paper
2001 QF_{298}	0.23 ± 0.09	0.16 ± 0.11	0.39 ± 0.11	This paper
(10370) Hylonome	0.18 ± 0.08	0.27 ± 0.09	0.45 ± 0.09	This paper
(15820) 1994 TB	0.38 ± 0.08	...	...	This paper
(26181) 1996 GQ_{21}	$0.48\pm0.07^{*}$	0.05 ± 0.08	$0.53\pm0.07^{*}$	This paper
(26375) 1999 DE_{9}	0.32 ± 0.11	-0.04 ± 0.11	0.28 ± 0.11	This paper
(33128) 1998 BU_{48}	0.52 ± 0.10	-0.19 ± 0.09	0.33 ± 0.10	This paper
(33340) 1998 VG_{44}	0.41 ± 0.06	0.01 ± 0.08	0.42 ± 0.08	This paper
(40314) 1999 KR_{16}	$0.58\pm0.06^{*}$	0.02 ± 0.07	$0.60\pm0.06^{*}$	This paper
(44594) 1999 OX_{3}	0.48 ± 0.07	-0.02 ± 0.09	0.46 ± 0.08	This paper
(52872) Okyrhoe	0.43 ± 0.09	0.16 ± 0.08	0.60 ± 0.07	This paper
(60558) 2000 EC_{98}	$0.56\pm0.06^{*}$	$0.34\pm0.06^{\ddagger}$	$0.90\pm0.05^{*,\ddagger}$	This paper
(66652) 1999 RZ_{253}	0.49 ± 0.09	0.10 ± 0.09	0.58 ± 0.06	This paper
(79360) 1997 CS_{29}	$0.38\pm0.08^{*}$	0.04 ± 0.08	$0.42\pm0.08^{*}$	This paper
Summary of the ESO Large Program *JHK* Photometry				
(26181) 1996 GQ_{21}	...	...	0.77 ± 0.06	Doressoundiram et al. (2003)
(26375) 1999 DE_{9}	0.29 ± 0.06	0.07 ± 0.06	0.36 ± 0.06	Doressoundiram et al. (2003)
(32532) Thereus	0.51 ± 0.04	0.11 ± 0.06	0.62 ± 0.06	Barucci et al. (2002)
(47171) 1999 TC_{36}	0.36 ± 0.06	-0.03 ± 0.07	0.33 ± 0.06	Dotto et al. (2003)
(52872) Okyrhoe	0.36 ± 0.05	0.20 ± 0.04	0.56 ± 0.05	Dotto et al. (2003)
(54598) Bienor	0.35 ± 0.06	0.14 ± 0.05	0.49 ± 0.05	Dotto et al. (2003)
(55565) 2002 AW_{97}	0.33 ± 0.04	0.23 ± 0.08	0.56 ± 0.08	Doressoundiram et al. (2006)
(55576) 2002 GB_{10}	0.29 ± 0.06	-0.08 ± 0.08	0.21 ± 0.06	Doressoundiram et al. (2006)
(63252) 2001 BL_{41}	0.37 ± 0.05	0.24 ± 0.06	0.61 ± 0.06	Doressoundiram et al. (2003)
(83982) 2002 GO_{9}	0.37 ± 0.06	-0.03 ± 0.07	0.34 ± 0.04	Doressoundiram et al. (2006)

Notes.—Indexes are computed from the magnitudes from Table 2 closest in time, apart from those computed (*) from the average of the J magnitudes, (†) from the average of the H magnitudes, and (‡) from the average of the K magnitudes available. Table 3 is also available in machine-readable form in the electronic edition of the *Astronomical Journal*.

distinction between the different subgroups commonly quoted: classical objects, resonant objects, scattered disk objects, extended scattered disk objects, and Centaurs.

For our color analysis, we adopt the same dynamical classification as in Doressoundiram et al. (2005). The dynamical type of the objects is set as follows: (1) Resonant objects are from Chiang et al. (2003). (2) Classical objects are the objects from the Minor Planet Center "Trans-Neptunian Objects" list with a semimajor axis 39.5 AU $< a <$ 48 AU (i.e., between the 3:2 and 2:1 resonances) and perihelion $q >$ 35 AU (i.e., outside Neptune's Hill sphere). Objects with $q >$ 36 AU and 36 AU $< a <$ 40 AU with low-inclination orbits with respect to the ecliptic plane are also stable and labeled as classical (Duncan et al. 1995). (3) Centaurs are the objects from the Minor Planet Center list "Centaurs and Scattered Disk Objects" with perihelia smaller than Neptune's semimajor axis (30 AU) and aphelia $Q <$ 48 AU (2:1 resonance). (4) SDOs are the objects left over after sorting out types 2 and 3. The resulting classification for our sample is listed in Table 4.

5.2. *The Visible–Near-IR Color Database*

We compiled the near-IR colors published in the literature to work on a larger sample for the use of statistical tools. This color compilation is made in the framework of the MBOSS (Minor Bodies of the Outer Solar System) database project first published in Hainaut & Delsanti (2002) and regularly updated. The current database is available online.[4] Table 4 contains the *VJHK* colors available for 51 objects. We also compiled previously published Bessel filter system *BRI* colors (for the sake of clarity, they do not appear in the table). We used and compiled the 1 σ errors published by the different authors. In the final average color index of a given object, each observer's contribution is weighted by $1/\sigma$, thus giving more weight to higher quality measurements. The error propagation is detailed in Hainaut & Delsanti (2002).

The resulting $J-H$ versus $H-K$ plot is shown in the left panel of Figure 1; a close up on Centaur colors is shown in the right panel. The star symbol shows the solar colors. The "reddening curve" drawn on the plot is described in Delsanti et al. (2004): it is the locus of objects with a reflectivity spectrum of increasing linear slope. The Sun, as a reference, has a linear reflectivity spectrum with a null slope. A tick mark is placed every 10%/100 nm; the curve is graduated in units of spectral slope from 0 (solar) to 70%/100 nm (very red). Most of the points lie below the reddening curve. This is an indication of a change and decrease of the spectral slope over the *JHK* range. Two outliers are apparent: (19308) 1996 TO_{66} (*top left point*) and (24835) 1995 SM_{55} (*bottom left point*). Object (19308) 1996 TO_{66} was measured by Jewitt & Luu (1998) and Davies et al. (2000). This

[4] See http://www.sc.eso.org/~ohainaut/MBOSS.

TABLE 4
COMPILATION OF PUBLISHED NEAR-IR COLORS

Object	Type[a]	$V-J\pm\sigma$	$J-H\pm\sigma$	$H-K\pm\sigma$	$J-K\pm\sigma$	Reference
1995 HM_5	3:2	...	1.20 ± 0.47	...	...	1
1996 TQ_{66}	3:2	2.43 ± 0.12	...	...	...	2
1996 TS_{66}	Classical	1.82 ± 0.17	0.65 ± 0.07	...	...	2, 3
1999 CD_{158}	Classical	1.86 ± 0.07	0.44 ± 0.10	0.03 ± 0.10	0.47 ± 0.09	4, 5
2000 KK_4	Classical	1.79 ± 0.10	...	...	...	6
2000 OJ_{67}	Classical	...	0.28 ± 0.09	0.07 ± 0.12	0.35 ± 0.12	5
2000 OK_{67}	Classical	2.42 ± 0.08	0.46 ± 0.08	0.04 ± 0.07	0.50 ± 0.09	4
2000 PE_{30}	SDO	...	0.42 ± 0.05	0.25 ± 0.07	0.67 ± 0.07	5
2001 CZ_{31}	Classical	...	0.55 ± 0.09	0.16 ± 0.09	0.71 ± 0.09	5
2001 QF_{298}	3:2	...	0.23 ± 0.09	0.16 ± 0.11	0.39 ± 0.11	5
(02060) Chiron	Centaur	1.20 ± 0.11	0.29 ± 0.08	0.06 ± 0.09	0.36 ± 0.08	7, 8, 9
(05145) Pholus	Centaur	2.61 ± 0.04	0.39 ± 0.04	−0.04 ± 0.04	0.35 ± 0.04	8, 9, 10, 11
(07066) Nessus	Centaur	2.29 ± 0.04	0.31 ± 0.26	−0.08 ± 0.38	0.31 ± 0.28	8, 9
(08405) Asbolus	Centaur	1.65 ± 0.04	0.39 ± 0.10	0.17 ± 0.17	0.59 ± 0.14	8, 9, 11, 12
(10199) Chariklo	Centaur	1.95 ± 0.34	0.48 ± 0.07	0.12 ± 0.05	0.56 ± 0.07	8, 9, 13
(10370) Hylonome	Centaur	1.31 ± 0.10	0.18 ± 0.08	0.27 ± 0.09	0.45 ± 0.09	5, 8
(15789) 1993 SC	3:2	2.43 ± 0.15	0.40 ± 0.20	−0.04 ± 0.19	0.36 ± 0.08	2, 3
(15820) 1994 TB	3:2	2.37 ± 0.16	0.41 ± 0.10	0.12 ± 0.12	0.57 ± 0.12	2, 4, 5
(15874) 1996 TL_{66}	SDO	1.45 ± 0.11	0.35 ± 0.11	−0.04 ± 0.11	0.31 ± 0.07	2, 3
(15875) 1996 TP_{66}	3:2	2.31 ± 0.06	0.17 ± 0.07	0.02 ± 0.09	0.19 ± 0.08	2, 3
(19308) 1996 TO_{66}	Classical	1.00 ± 0.10	−0.21 ± 0.17	0.81 ± 0.15	0.60 ± 0.09	2, 3
(19521) Chaos	Classical	1.83 ± 0.08	0.40 ± 0.05	0.02 ± 0.05	0.42 ± 0.05	2, 4
(20000) Varuna	Classical	2.01 ± 0.05	...	...	...	6
(24835) 1995 SM_{55}	Classical	1.02 ± 0.05	−0.49 ± 0.06	−0.09 ± 0.07	−0.57 ± 0.07	4, 6
(26181) 1996 GQ_{21}	SDO	2.44 ± 0.06	0.48 ± 0.07	0.05 ± 0.08	0.68 ± 0.11	5, 6, 14
(26308) 1998 SM_{165}	2:1	2.37 ± 0.06	0.52 ± 0.08	0.08 ± 0.07	0.60 ± 0.08	4, 6
(26375) 1999 DE_9	SDO	1.89 ± 0.06	0.30 ± 0.08	0.01 ± 0.10	0.32 ± 0.09	5, 6, 14
(29981) 1999 TD_{10}	SDO	1.79 ± 0.05	...	...	...	6
(31824) Elatus	Centaur	...	...	0.02 ± 0.08	...	4
(32532) Thereus	Centaur	...	...	0.11 ± 0.06	...	15
(32929) 1995 QY_9	3:2	2.03 ± 0.20	...	...	...	2
(33128) 1998 BU_{48}	Centaur	2.27 ± 0.05	0.50 ± 0.09	−0.16 ± 0.10	0.35 ± 0.09	4, 5
(33340) 1998 VG_{44}	3:2	...	0.41 ± 0.06	0.01 ± 0.08	0.42 ± 0.08	5
(35671) 1998 SN_{165}	Classical	1.27 ± 0.05	...	...	...	6
(38628) Huya	3:2	1.97 ± 0.05	...	...	...	6
(40314) 1999 KR_{16}	SDO	...	0.58 ± 0.06	0.02 ± 0.07	0.60 ± 0.06	5
(44594) 1999 OX_3	Centaur	2.11 ± 0.08	0.48 ± 0.07	−0.02 ± 0.09	0.45 ± 0.08	5, 6
(47171) 1999 TC_{36}	3:2	2.33 ± 0.06	0.36 ± 0.08	−0.03 ± 0.07	0.36 ± 0.08	4, 6, 16
(47932) 2000 GN_{171}	3:2	1.76 ± 0.06	...	...	...	6
(48639) 1995 TL_8	SDO	2.42 ± 0.05	0.40 ± 0.07	−0.02 ± 0.08	0.38 ± 0.07	4
(52872) Okyrhoe	Centaur	...	0.41 ± 0.07	0.16 ± 0.08	0.58 ± 0.06	5, 16
(52975) Cyllarus	Centaur	2.42 ± 0.07	0.45 ± 0.09	−0.10 ± 0.08	0.35 ± 0.09	4
(54598) Bienor	Centaur	1.69 ± 0.06	0.39 ± 0.09	0.18 ± 0.08	0.58 ± 0.14	4, 16
(55565) 2002 AW_{197}	Classical	...	0.32 ± 0.06	0.27 ± 0.06	0.59 ± 0.06	17
(55576) 2002 GB_{10}	Centaur	...	0.30 ± 0.08	0.00 ± 0.06	0.30 ± 0.08	17
(60558) 2000 EC_{98}	Centaur	...	0.56 ± 0.06	0.34 ± 0.06	0.90 ± 0.05	5
(63252) 2001 BL_{41}	Centaur	...	0.36 ± 0.07	0.25 ± 0.10	0.62 ± 0.09	14
(66652) 1999 RZ_{253}	Classical	2.01 ± 0.06	0.48 ± 0.09	0.10 ± 0.09	0.58 ± 0.06	5, 6
(79360) 1997 CS_{29}	Classical	2.07 ± 0.13	0.35 ± 0.12	0.00 ± 0.15	0.36 ± 0.16	1, 2, 5
(83982) 2002 GO_{09}	Centaur	...	0.37 ± 0.05	−0.14 ± 0.06	0.33 ± 0.10	17
(91133) 1998 HK_{151}	3:2	1.57 ± 0.09	...	...	...	6

NOTES.—This is a compilation of colors averaged from different observers. Only colors computed from simultaneous photometry (both filters observed within a couple of hours) are used. Some differences are noticed from Table 3, which reports colors as published by their authors [for example, (32532) Thereus]. Table 4 is also available in machine-readable form in the electronic edition of the *Astronomical Journal*.

[a] SDO = scattered disk object, 3:2 and 2:1 = resonant objects.

REFERENCES.—(1) Boehnhardt et al. 2001; (2) Davies et al. 2000; (3) Jewitt & Luu 1998; (4) Delsanti et al. 2004; (5) this paper; (6) McBride et al. 2003; (7) Hartmann et al. 1981; (8) Davies 2000; (9) Davies et al. 1998; (10) Davies et al. 1993; (11) Weintraub et al. 1997; (12) Romon-Martin et al. 2002; (13) McBride et al. 1999; (14) Doressoundiram et al. 2003; (15) Barucci et al. 2002; (16) Dotto et al. 2003; (17) Doressoundiram et al. 2006.

blue object was reported to have a nonrepeatable visible light curve over time (Hainaut et al. 2000; Sekiguchi et al. 2002) in amplitude, shape, and rotation period. Sheppard & Jewitt (2003) later showed that only the light-curve amplitude might be varying. This result is confirmed by Belskaya et al. (2005). They match the amplitude increases with opposition surge effects that occur at small phase angles. Belskaya et al. also argue that phase-angle effects are most probably responsible for the problems in determining an unambiguous rotation period. Object (24835) 1995 SM_{55} was measured by McBride et al. (2003) and Delsanti et al.

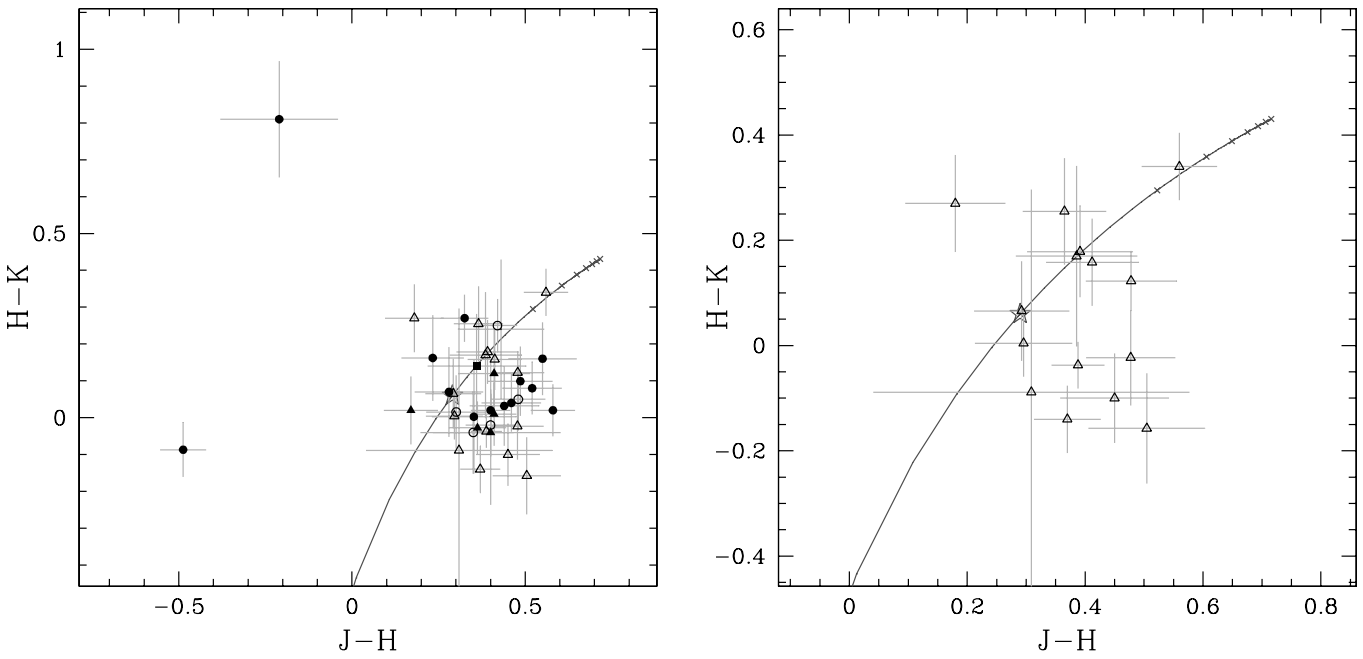

FIG. 1.—$J - H$ vs. $H - K$ colors. Shown are resonant objects (*filled triangles*), classical objects (*filled circles*), centaurs (*open triangles*), SDOs (*open circles*), and the Sun (*star*). The curve is the locus of objects with a linear reflectivity spectrum over the $J \rightarrow K$ range (see § 5.2). *Left*: Top left point is object (19308) 1996 TO_{66}; bottom left point is (24835) 1995 SM_{55}. *Right*: Close-up of Centaur colors only. [*See the electronic edition of the Journal for a color version of this figure.*]

(2004). The latter published a noticeably blue reflectivity spectrum (especially in the near-IR), which might be an indication of the presence, for example, of water ice (broad absorption band around 2 μm). Unfortunately, this target is too faint to be observed with near-IR spectroscopy. According to Sheppard & Jewitt (2003), 1995 SM_{55} has a nonrepeatable visible light curve over time. Several causes are suggested: the presence of an unresolved companion, cometary activity, or—less likely—a complex rotational state.

6. DISCUSSION

6.1. *Color-Color Correlations*

In this section we compare the different color samples (*BVRIJHK* and visible gradient S) two by two using the Spearman rank correlation (Spearman 1904). Spearman correlation does not require that KBOs and Centaur color distributions be Gaussian; it is distribution-free and able to provide meaningful significance levels even for small samples of objects. The method also takes into account the error bars of the measurements. We discuss those results with a correlation coefficient ρ greater than $\sim$0.60 in absolute value. The significance level associated with the correlation coefficient ρ gives the level of evidence against the null hypothesis H_0, which is, *the two samples are not correlated*. Based on the conventions of Efron & Tibshirani (2003), we interpret the results as (1) SL (significance level) > 95%, reasonably strong evidence against H_0; (2) SL > 97.5%, strong evidence against H_0; and (3) SL > 99.7%, very strong evidence against H_0 (canonical 3 σ Gaussian probability).

Table 5 shows a qualitative summary of the results for all dynamical types and significance levels. The corresponding correlation coefficients and significance levels are listed in Table 6. In this section we discuss only the most relevant results.

6.1.1. *The Centaurs*

Results at the 3 σ significance level.—There is a strong correlation between the $B - V$ and $V - J$ indexes (see top part of Table 6). The two indexes are thus related by a monotonic

TABLE 5
QUALITATIVE SUMMARY OF COLOR-COLOR CORRELATIONS

	3 σ SL[a]		97.50% < SL ≤ 99.73%		95.0% < SL ≤ 97.5%	
TYPE	n[b]	Correlation	n	Correlation	n	Correlation
Centaur	10	$B - V$ vs. $V - J$, $V - H$, $V - K$	10	$V - J$, $V - H$, $V - K$ vs. visible colors and S[c]	10	$V - J$, $V - H$ vs. $H - K$
	...	...	17	$H - K$ vs. visible colors and S	...	...
Classical	...	No result	7	$V - J$ vs. $V - K$	11	$V - J$ vs. visible colors and S
	...	...	8	$V - J$ vs. $V - H$	...	...
	...	...	7	$V - H$ vs. $V - K$	...	...
Resonant	...	No result	9	$V - J$ vs. S	9	$V - J$ vs. $B - V$, $R - I$
Scattered disk	...	No result	...	No result	...	No result

NOTE.—Corresponding correlation coefficients are listed in Table 6.
[a] Significance level of the correlation coefficient.
[b] Number of objects for this correlation.
[c] Visible gradient.

TABLE 6

COLOR-COLOR CORRELATIONS

TYPE	SL ≥ 99.73 (3 σ LEVEL)					97.50 < SL ≤ 99.73					95.0 < SL ≤ 97.5				
	Correlation	n[a]	$\langle\rho\rangle_{-\sigma}^{+\sigma}$[b]	SL[c]	σ_{SL}	Correlation	n	$\langle\rho\rangle_{-\sigma}^{+\sigma}$	SL	σ_{SL}	Correlation	n	$\langle\rho\rangle_{-\sigma}^{+\sigma}$	SL	σ_{SL}
Centaur	$V-J$ vs. $B-V$	10	$0.88^{+0.05}_{-0.09}$	99.92	3.35	$V-J$ vs. $V-R$	10	$0.82^{+0.08}_{-0.13}$	99.64	2.91	$V-J$ vs. $H-K$	10	$-0.66^{+0.17}_{-0.12}$	96.08	2.06
	$V-J$ vs. S	10	$0.87^{+0.05}_{-0.09}$	99.90	3.29	$V-J$ vs. $R-I$	10	$0.82^{+0.09}_{-0.18}$	99.66	2.92	$H-K$ vs. $V-H$	10	$-0.67^{+0.18}_{-0.13}$	96.67	2.13
	$V-J$ vs. $V-H$	10	$0.94^{+0.03}_{-0.06}$	99.99	4.04	$V-J$ vs. $I-J$	9	$0.78^{+0.09}_{-0.15}$	98.69	2.48	$B-V$ vs. $I-J$	9	$0.67^{+0.13}_{-0.19}$	95.09	1.97
	$V-J$ vs. $V-K$	10	$0.91^{+0.04}_{-0.09}$	99.98	3.70		...	...	...	...	...	...	...	...	...
	...	...	...	...	...	$H-K$ vs. $B-V$	17	$-0.64^{+0.12}_{-0.09}$	99.42	2.76	...	...	...	...	...
	$V-H$ vs. $B-V$	10	$0.86^{+0.06}_{-0.10}$	99.87	3.22	$H-K$ vs. $V-R$	17	$-0.62^{+0.15}_{-0.11}$	99.15	2.63	...	...	...	...	...
	$V-H$ vs. $V-K$	10	$0.89^{+0.05}_{-0.10}$	99.95	3.48	$H-K$ vs. $R-I$	17	$-0.59^{+0.18}_{-0.13}$	98.67	2.48	...	...	...	...	...
	...	...	...	...	...	$H-K$ vs. S	17	$-0.64^{+0.13}_{-0.10}$	99.40	2.75	...	...	...	...	...
	$V-K$ vs. $B-V$	10	$0.83^{+0.07}_{-0.12}$	99.73	3.00	$H-K$ vs. $J-K$	15	$0.62^{+0.13}_{-0.18}$	98.72	2.49	...	...	...	...	...
	...	...	...	...	...	$V-H$ vs. $V-R$	10	$0.78^{+0.10}_{-0.16}$	99.15	2.63	...	...	...	...	...
	...	...	...	...	...	$V-H$ vs. $R-I$	10	$0.79^{+0.11}_{-0.20}$	99.37	2.73	...	...	...	...	...
	...	...	...	...	...	$V-H$ vs. $I-J$	9	$0.81^{+0.09}_{-0.15}$	99.17	2.64	...	...	...	...	...
	...	...	...	...	...	$V-H$ vs. S	10	$0.83^{+0.07}_{-0.12}$	99.71	2.98	...	...	...	...	...
	...	...	...	...	...	$V-K$ vs. $V-R$	10	$0.77^{+0.11}_{-0.18}$	99.07	2.60	...	...	...	...	...
	...	...	...	...	...	$V-K$ vs. $R-I$	10	$0.77^{+0.11}_{-0.20}$	99.07	2.60	...	...	...	...	...
	...	...	...	...	...	$V-K$ vs. $I-J$	9	$0.78^{+0.10}_{-0.16}$	98.72	2.49	...	...	...	...	...
	...	...	...	...	...	$V-K$ vs. S	10	$0.82^{+0.09}_{-0.15}$	99.66	2.93	...	...	...	...	...
	...	...	...	...	...	$H-K$ vs. Q	17	$-0.57^{+0.12}_{-0.10}$	98.42	2.41	$J-K$ vs. a	15	$-0.57^{+0.13}_{-0.11}$	97.28	2.21
	...	...	...	...	...	$J-K$ vs. Q	15	$-0.58^{+0.14}_{-0.11}$	97.65	2.27	...	...	...	...	...
	...	...	...	...	...	$H-K$ vs. a	17	$-0.55^{+0.11}_{-0.09}$	97.82	2.29	...	...	...	...	...
Classical	...	...	...	...	...	$V-H$ vs. $V-K$	7	$0.91^{+0.05}_{-0.09}$	99.56	2.85	$V-J$ vs. S	11	$0.65^{+0.11}_{-0.16}$	97.05	2.18
	...	...	...	...	...	$V-J$ vs. $V-K$	7	$0.90^{+0.05}_{-0.09}$	99.47	2.79	$V-J$ vs. $V-R$	11	$0.63^{+0.14}_{-0.19}$	96.38	2.09
	...	...	...	...	...	$V-J$ vs. $V-H$	8	$0.84^{+0.08}_{-0.16}$	99.17	2.64	$V-J$ vs. $R-I$	10	$0.65^{+0.15}_{-0.22}$	95.76	2.03
	...	...	...	...	...	...	...	...	...	...	$J-H$ vs. $V-K$	7	$0.76^{+0.12}_{-0.22}$	95.27	1.98
	...	...	...	...	...	$V-H$ vs. H	8	$0.88^{+0.06}_{-0.13}$	99.61	2.89	$V-H$ vs. i	8	$-0.77^{+0.12}_{-0.08}$	97.45	2.23
	...	...	...	...	...	$V-K$ vs. H	7	$0.92^{+0.04}_{-0.08}$	99.66	2.93	$V-K$ vs. i	7	$-0.78^{+0.08}_{-0.06}$	96.21	2.08
	...	...	...	...	...	$V-J$ vs. q	11	$0.67^{+0.08}_{-0.09}$	97.62	2.26	$V-H$ vs. E	8	$-0.76^{+0.15}_{-0.10}$	97.04	2.17
	...	...	...	...	...	...	...	...	...	...	$V-J$ vs. E	11	$-0.60^{+0.08}_{-0.07}$	95.08	1.97
	...	...	...	...	...	...	...	...	...	...	$V-J$ vs. a	11	$0.62^{+0.08}_{-0.09}$	95.85	2.04
Resonant	...	...	...	...	...	$V-J$ vs. S	9	$0.74^{+0.12}_{-0.18}$	97.60	2.26	$V-J$ vs. $B-V$	9	$0.70^{+0.14}_{-0.23}$	96.37	2.09
	...	...	...	...	...	...	...	...	...	...	$V-J$ vs. $R-I$	9	$0.68^{+0.15}_{-0.23}$	95.64	2.02
	...	...	...	...	...	...	...	...	...	...	$V-J$ vs. a	9	$-0.72^{0.10}_{-0.08}$	97.04	2.17

[a] Number of objects in the sample studied.

[b] Spearman rank correlation coefficient and 1 σ errors.

[c] Significance level of ρ.

function (which is not necessary linear). In Figure 2 (*top left*) the data points follow the reddening curve quoted in § 5.2 rather well. This curve might be in turn the monotonic function that relates the $B - V$ and $V - J$ indexes. This means that the Centaurs display a quasi-linear reflectivity spectrum over the $V \rightarrow J$ range. This result was mentioned in McBride et al. (2003) and Delsanti et al. (2004), for both KBOs and Centaurs. Logically, a strong correlation also appears between $V - J$ and the visible gradient S.

The $B - V$ index also correlates with $V - H$ and $V - K$, with slightly lower ρ and significance levels. The relation between these indexes looks rather linear (see Fig. 2, *top right and bottom left*). The Centaurs with redder visible colors also have redder $V - H$ and $V - K$ indexes, with a flattening of the spectral slope in the infrared range (red data points are located below the reddening curve). These correlations indicate that the same process is most probably responsible for the surface color behavior in the visible–near-IR range. Other results in the top part of Table 6 confirm this conclusion.

Results with SL $> 97.5\%$.—The most interesting result is the dependency of $H - K$ on the visible indexes ($B - V$, $V - R$, $R - I$, and the visible gradient S; see Table 6). Although the correlation coefficient ρ is slightly above 0.60 (the correlation is visually quite broad), an interesting result appears: the far end of the near-IR reflectivity spectrum ($H - K$ region) is bluer for visually redder objects. This result clearly appears on the $B - V$ versus $H - K$ diagram (Fig. 3, *left*). The Centaurs that have an $H - K$ color bluer than the Sun (*bottom right quadrant*) are systematically the reddest objects in the visible range. On normalized reflectivity spectra, these objects have the largest visible gradients, along with a negative spectral slope over the $H \rightarrow K$ ($\sim$1.6–2.2 μm) range. This might be a hint of the presence of a solid state absorption band longward of 1.7 μm. Only a proper spectroscopic study can unveil the nature of the chemical component causing this feature. In theory, several ices may produce such a reflectance spectrum in the $H - K$ region: water ice (broad absorption band around 2 μm), CH_4, NH_3, etc., although the relative depth of the absorption features is closely related to the quantity of ice present on the surface. Silicates are also known to show some absorptions in the 2 μm region. Titan tholins (a synthetic involatile material obtained by irradiation of a gas mixture of N_2 and CH_4 and used to describe the aerosols on the surface of Titan [Khare et al. 1984; Sagan et al. 1984; Imanaka et al. 2004]) have a steep visible spectrum and display a broad depression around 2 μm.

The objects in our sample that have $H - K$ colors bluer than the Sun are (by increasing value of $H - K$) (33128) 1998 BU_{48}, (83982) 2002 GO_9, (52925) Cyllarus, (7066) Nessus, (5145) Pholus, (44594) 1999 OX_3, (55576) 2002 GB_{10}, and (31824) Elatus. As regards real IR spectroscopic studies, (55576) 2002 GB_{10} and (83982) 2002 GO_9 were observed by Doressoundiram et al. (2006). Water is unambiguously detected for the latter object. The IR spectrum of (55576) 2002 GB_{10} is more difficult to interpret. The composition model presented suggests that the surface of this object is 33% contaminated water ice. Several works reported the presence of water ice on Pholus (Cruikshank et al. 1998; Brown 2000). Titan tholins have also been invoked to describe its surface composition. Nessus has never been observed with infrared spectroscopy, nor have the other objects. In turn, this trend points toward Centaurs, which could harbor water on their surface (among other possibilities), a hypothesis that could be observationally tested. We checked the orbital parameters of these eight objects to see whether they share some common characteristics. No pattern was identified.

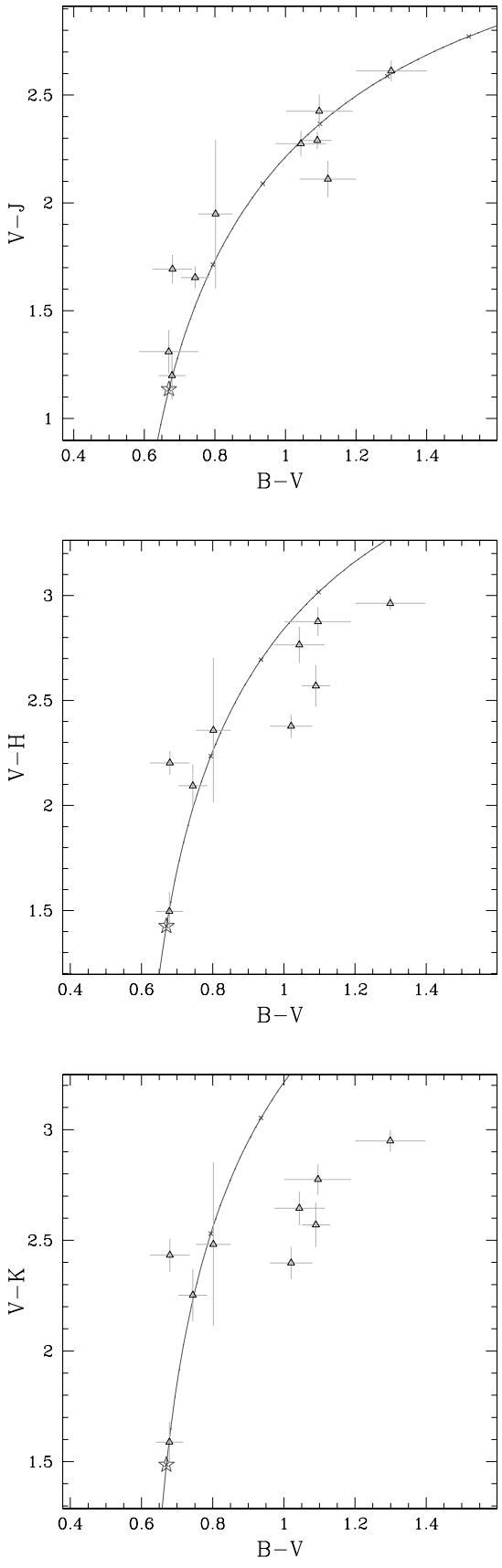

FIG. 2.—Visible–near-IR colors of Centaurs. Solar colors are marked with a star; the curve is the reddening curve, the locus of objects with a linear reflectivity spectrum. [*See the electronic edition of the Journal for a color version of this figure.*]

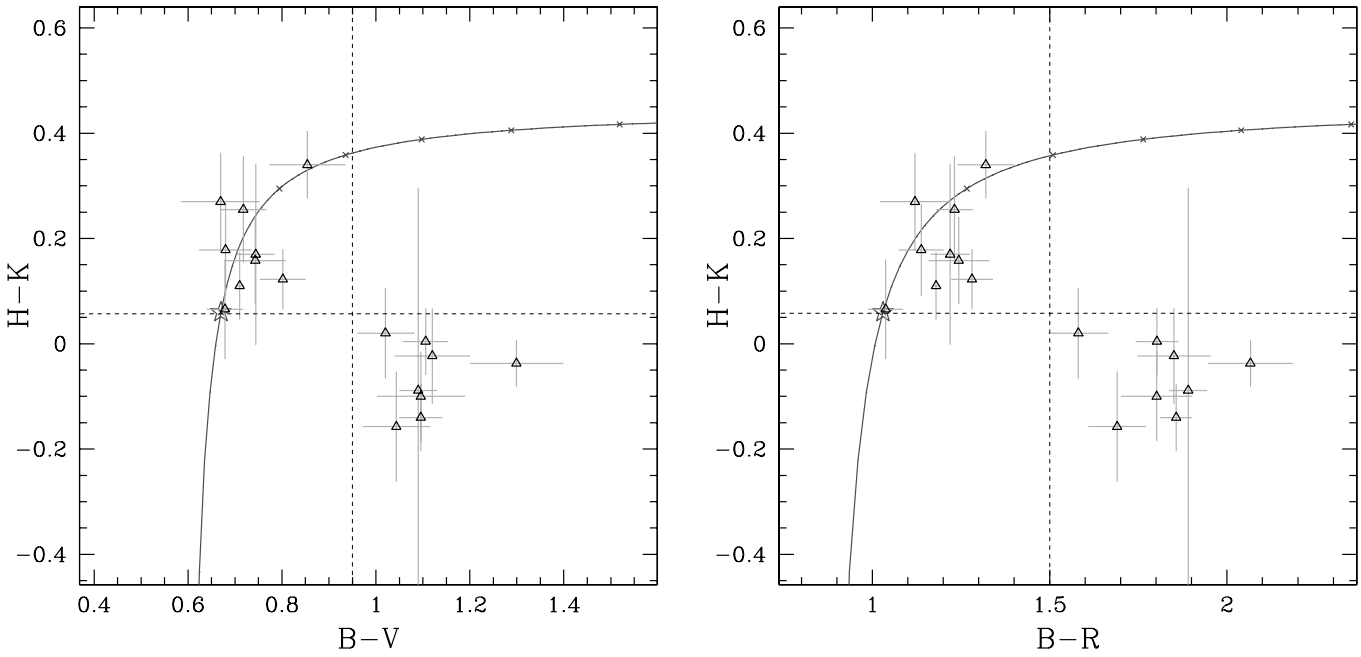

FIG. 3.—$B - V$ vs. $H - K$ and $B - R$ vs. $H - K$ color diagrams for Centaurs. Conventions are the same as in Fig. 1. The horizontal dashed line shows the solar $H - K$ value; the vertical dashed line is arbitrarily set to guide the eye. [*See the electronic edition of the Journal for a color version of this figure.*]

Results at the SL > 95% *level*.—These are consistent with what has been described above. The $V - J$ versus $H - K$ correlation confirms that the Centaurs with $H - K$ bluer than the Sun have systematically the reddest $V - J$ colors (Table 6).

6.1.2. *Classical KBOs and Other Objects*

There are no 3 σ level correlations for the classical KBOs' colors (Table 6). At the lower SL > 97.5% level, the $V - J$, $V - H$, and $V - K$ colors are positively correlated ($\rho > 0.84$). As for Centaurs, this result implies that the same coloring process is acting on both the visible and near-IR colors. Correlations at the next level (SL > 95%) are consistent with this result.

We found no significant results (i.e., SL > 95%) for the current sample (seven objects) of SDO near-IR colors. As regards the resonant objects (nine objects), we have a correlation between $V - J$ and visible gradient S, $B - V$, and $R - I$ at significance levels of 97.6% and lower (Table 6). Again, this implies that a single coloring agent is probably acting on the visible–near-IR colors.

6.2. *Color–Physical Parameter Correlations*

We also tested all combinations of color indexes with physical parameters: the orbital semimajor axis a, inclination with respect to the ecliptic plane i, eccentricity e and energy E [defined as $(e^2 + \sin^2 i)^{1/2}$], perihelion q and aphelion Q, absolute magnitude $M(1, 1)$ [computed as $M(1, 1) = R - 5 \log(r\Delta)$, with r and Δ being the geo- and heliocentric distances in AU, respectively]. In our tables and below, $M(1, 1)$ is more compactly denoted H. In this study, we did not take into account the phase effects: the maximum measured opposition effects are of the order of a few tenths of magnitude and therefore should not dramatically influence correlations. We also tested the possible correlations of H with the orbital parameters. For all dynamical subclasses, there are no 3 σ level correlations. In this section we briefly mention the other results. Table 7 gives a qualitative overview of the trends; correlation coefficients are given in Table 6.

At the SL > 97.5% level, Centaur $H - K$ and $J - K$ colors show some hints of a correlation with the aphelion distance Q for 17 and 15 objects, respectively (see top part of Table 6). However, the absolute value of the ρ coefficient is slightly lower than 0.60, which means that the correlation is extremely broad.

As regards classical KBOs, the $V - K$ (seven objects) and $V - H$ (eight objects) indexes show a quite strong correlation with absolute magnitude H (Table 6): intrinsically brighter objects show bluer visible–infrared colors than fainter objects. This

TABLE 7
QUALITATIVE SUMMARY OF COLOR–PHYSICAL PARAMETER CORRELATIONS

	3 σ SL[a]		97.50 < SL ≤ 99.73		95.0 < SL ≤ 97.5	
TYPE	n[b]	Correlation	n	Correlation	n	Correlation
Centaur	...	No result	17	$H - K$ vs. Q ?	15	$J - K$ vs. a ?
	...	...	15	$J - K$ vs. Q ?	...	...
Classical	...	No result	8	$V - H$ vs. H	8	$V - H$ vs. i, E
	...	...	7	$V - K$ vs. H	7	$V - K$ vs. i
	...	...	11	$V - J$ vs. q	11	$V - J$ vs. a, E
Resonant	...	No result	...	No result	9	$V - J$ vs. a
Scattered disk	...	No result	...	No result	...	No result

NOTES.—Corresponding correlation coefficients are listed in Table 6. A question mark indicates broad correlations (ρ slightly lower than 0.60).

[a] Significance level of the correlation coefficient.

[b] Number of objects for this correlation.

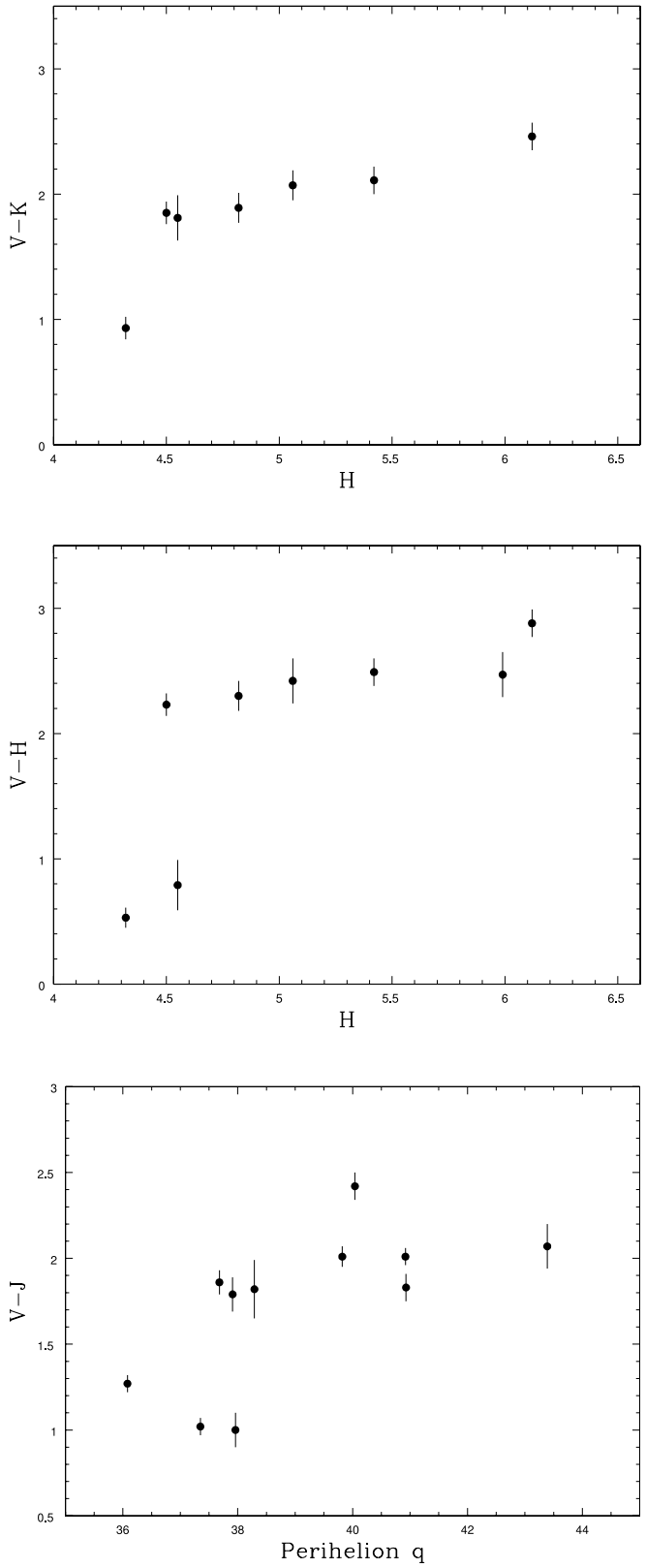

FIG. 4.—Color vs. absolute magnitude and color vs. perihelion distance trends for visible–near-IR colors of classical objects.

result had already been reported for visible colors in Hainaut & Delsanti (2002). Usually, absolute magnitude is used as a hint for the size of the objects. It is related to the product of the square diameter and the albedo of the object. KBO albedos are known for a few bright objects, but without albedo measurements, there is no way to rigorously estimate object diameters. The alternate solution is to assume an albedo value and derive an estimate of the diameter. Given the range of the currently known visible albedos for classical KBOs (from 4% to 40%; Grundy et al. 2005), the estimated diameter can be wrong by a factor of up to 3, depending on how far the chosen value is from the real (unknown) value. If we assume a common albedo for all objects of the sample (which is a priori not guaranteed), the previous result might be translated as "bigger objects show bluer colors than smaller objects." In the context of the resurfacing model developed by Delsanti et al. (2004), cometary activity produces uniform neutral surfaces by redeposition of neutral-colored suborbital dust subsequent to the outgassing. However, only the biggest objects can retain this dust and be resurfaced. Thus, bigger objects show bluer colors, which is consistent with the trend above. However, this hypothesis remains speculative: there is no observational evidence for a surface albedo homogeneity or routine cometary activity among classical KBOs. From the top and middle plots in Figure 4, these correlations appear to be driven by the presence of the two very blue objects, the outliers 1999 SM_{55} and 1996 TO_{66} mentioned in § 5.2. After removing these two objects, the correlations decrease drastically in significance level. As a conclusion, this result is interesting enough to be mentioned, but it needs to be confirmed with more data points.

Classical KBOs also show a broad correlation between $V - J$ and perihelion distance q for 11 objects (Fig. 4, *bottom*). This result, although not extremely significant (Table 6), is consistent with findings for the visible colors (Doressoundiram et al. 2005) and should be monitored on a growing color sample. The same applies to the various low significance level correlations found with inclination and orbital energy that are consistent with results on visible colors by Trujillo & Brown (2002), Doressoundiram et al. (2002), and Hainaut & Delsanti (2002).

The SDOs' near-IR colors (seven objects) do not show any correlation with the orbital parameters or absolute magnitude with a significance level greater than 90%. The $V - J$ colors of the nine resonant objects correlate with the semimajor axis at a very marginal level.

6.3. *Are Centaur Visible–Near-IR Color Distributions Bimodal?*

From the very first KBO photometric studies, a controversy has arisen over a possible bimodal structure of the visible color distributions of the whole KBO and Centaur population. Indeed, Tegler & Romanishin (1998, 2000, 2003) claimed two separate groups of objects from their data set: one with neutral (solar) colors, the other with very red colors. Peixinho et al. (2003) showed that this structure appears only among the Centaur population for some visible colors. They performed a "dip test" (see § 6.3.2) on a sample of 20 Centaurs and found a 99.5% confidence level for a bimodal structure of the $B - R$ distribution and 97.7% for the $V - R$ distribution. This result was confirmed when testing the Tegler and Romanishin samples of Centaurs alone (while the KBO sample from their paper did not show any statistically significant bimodality, as shown by Peixinho et al. 2003). On the other hand, Bauer et al. (2003) found no bimodal structure in their data set of 24 Centaurs. However, their work sampled *VRI* colors, whereas the bimodal structure is found by Peixinho et al. to appear most strongly in the $B - R$ index. In this work, we

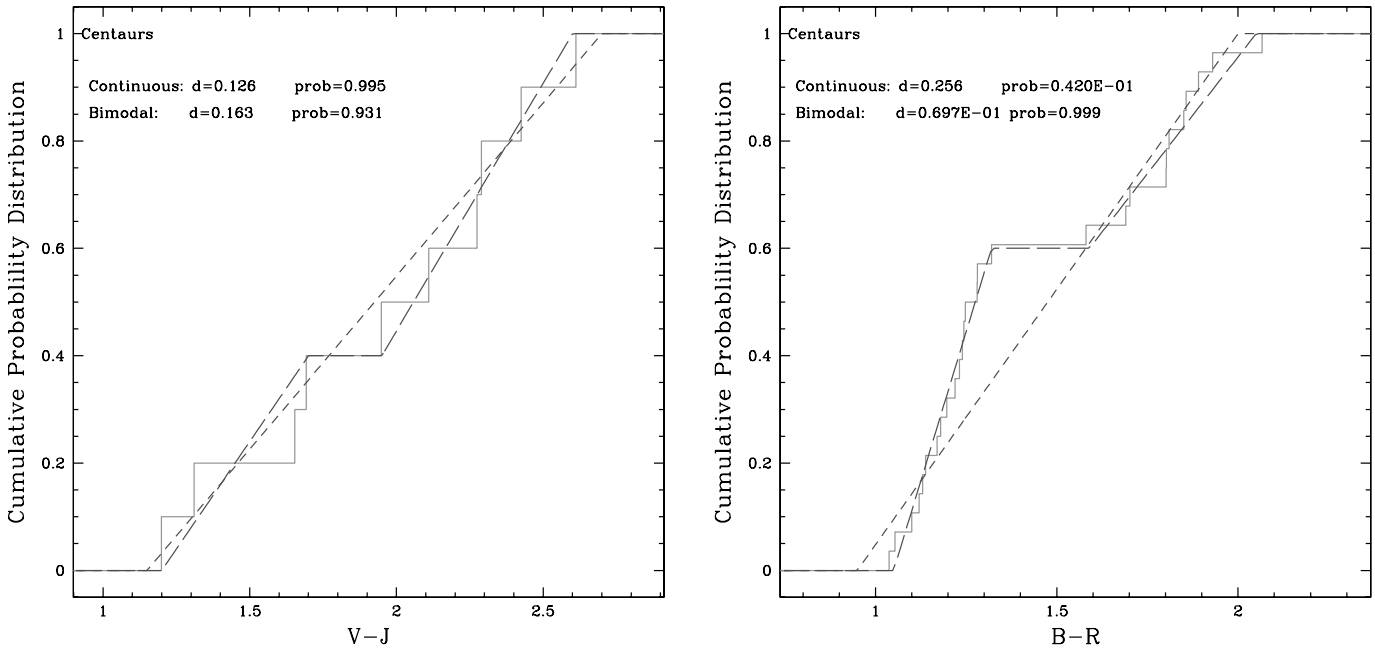

FIG. 5.—Cumulative probability functions of the Centaur $V - J$ colors compared to a continuous and a bimodal (case of $F = 0.40$) model distribution that maximizes the K-S statistic's probability (*left*). The same is shown for the visible $B - R$ color distribution (*right*). [*See the electronic edition of the Journal for a color version of this figure.*]

investigate the structure of the near-IR color distributions of Centaurs on a sample of up to 17 objects (*JHK* colors). We also monitor the structure of the corresponding *BVRI* colors. We use two statistical tools: the Kolmogorov-Smirnov (K-S) test and the dip test.

6.3.1. *The Kolmogorov-Smirnov Test*

The $J - H$ versus $H - K$ color-color diagram visually displays no obvious bimodal structure (see Fig. 1, *right*). To quantify this, we use the K-S method to test the color distribution structure. We compare the observed one-dimensional color distributions to very simple models of bimodal and unimodal color distributions. The K-S test (Kolmogorov 1933) estimates the maximum vertical distance d between the cumulative probability functions of two one-dimensional distributions. This distance d is converted into the probability of the two distributions being drawn from the same parent distribution. Low probability values (e.g., a few percent) indicate that the two distributions are statistically incompatible. Large values only indicate that the two distributions are *not* statistically incompatible, but in no case prove that the distributions are drawn from the same parent distribution. We therefore compared some of the observed one-dimensional distributions ($V - J, J - H, H - K$, and $J - K$, but also the visible colors for reference) with a simple model of continuous and bimodal distributions (see Fig. 5, *left*, for index $V - J$) that were adjusted to the data to maximize the probability. The details on how the different one-dimensional continuous and bimodal synthetic best-fitting distributions are built are described in Hainaut & Delsanti (2002).

Table 8 lists the corresponding results for distance d and probability. For bimodal model distributions, F is the fraction of objects contained in the "bluer" group. The $V - J$ (10 objects), $J - H$ and $J - K$ (15 objects), and $H - K$ (17 objects) color distributions show no statistically significant evidence for a bimodal structure. The $H - K$ distribution shows some significant evidence (probability >99.99%) for a continuous structure. We also tested the visible color distributions of this present sample. We found that the $B - R$ index shows statistically significant evidence for a bimodal structure with a probability of 99.9% (see Fig. 6 and the cumulative probability function in Fig. 5, *right*). This is compatible with the result reported in Peixinho et al. (2003) on different data. More precisely, the present data sample contains 16 objects in common with Peixinho et al. (with *BVR* colors compiled from both a larger and more recent set of papers) plus (32532) Thereus.

TABLE 8
CENTAUR COLOR BIMODALITY: THE KOLMOGOROV-SMIRNOV TESTS

Color	n[a]	Model	F[b]	d	Probability (%)
$J - H$	15	Continuous	...	0.128	95.3
		Bimodal	0.26	0.234	33.9
$H - K$	17	Continuous	...	0.082	>99.99
		Bimodal	0.48	0.270	14.1
$J - K$	15	Continuous	...	0.211	46.9
		Bimodal	0.46	0.265	20.6
$V - J$	10	Continuous	...	0.126	99.5
		Bimodal	0.20	0.164	92.9
		Bimodal	0.40	0.163	93.1
$B - V$	17	Continuous	...	0.213	13.9
		Bimodal	0.60	0.127	73.1
$B - R$	17	Continuous	...	0.256	4.2
		Bimodal	0.60	0.069	99.9
$V - J$ vs. $J - H$	10	Continuous	...	0.188	88.0
		Bimodal	0.20	0.213	76.5
$V - J$ vs. $J - K$	10	Continuous	...	0.181	90.5
		Bimodal	0.20	0.256	54.4
$J - H$ vs. $H - K$	15	Continuous	...	0.161	87.9
		Bimodal	0.50	0.254	34.9
$B - V$ vs. $H - K$	17	Continuous	...	0.267	21.6
		Bimodal	0.50	0.131	95.1
$B - R$ vs. $H - K$	17	Continuous	...	0.268	21.4
		Bimodal	0.50	0.126	96.4

[a] Number of objects in the sample studied.
[b] Fraction of objects in the first (blue) group.

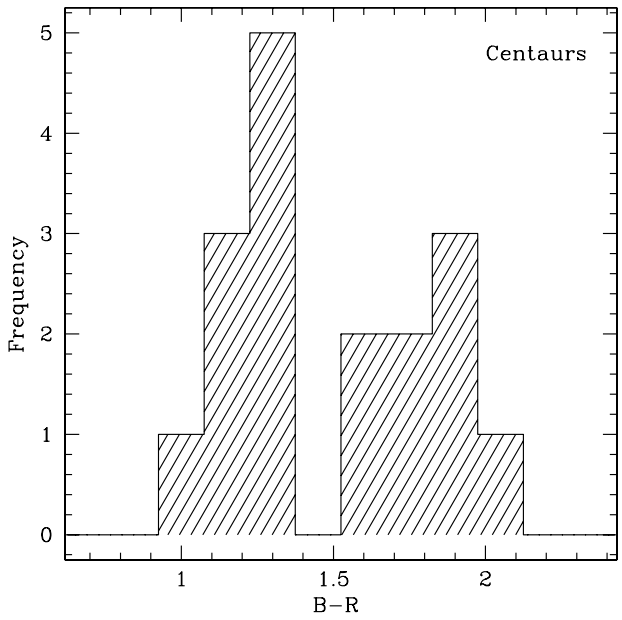

FIG. 6.—Histogram of the $B - R$ colors for the 17 Centaurs studied in this work.

We also used the two-dimensional version of the K-S test (Peacock 1983; Fasano & Franceschini 1987) to probe the structure of some of the color-color diagrams. For example, the $B - V$ versus $H - K$ and $B - R$ versus $H - K$ diagrams (Fig. 3) visually display a bimodal structure. This result is not statistically significant (Table 8), although in the $B - R$ versus $H - K$ space the bimodal case reaches a significance level of up to 96.4%. All the results are listed in Table 8. No probability value lies below a few percent, which means that the observed two-dimensional distributions tested are not statistically incompatible with a continuous or bimodal distribution.

6.3.2. *The Dip Test*

This test was designed by Hartigan & Hartigan (1985) to unveil the presence of more than one group in a distribution. The dip statistic is the maximum difference between the studied distribution and the unimodal synthetic distribution that minimizes that maximum difference. In turn, this test is very similar to the K-S test used above, except that the dip test finds the unimodal distribution itself by a best-fitting algorithm (whereas in the K-S test, the user has to find this best-fitting distribution). The dip quantity is close to zero for samples that are drawn from a unimodal distribution. The probability that the computed dip value is not obtained by chance is available in tables by Hartigan & Hartigan (1985). The results of the dip test for our sample are displayed in Table 9. They confirm the results obtained with the K-S test: the *JHK* colors show no statistical evidence for a bimodal structure.

As regards the visible indexes, the dip test reveals bimodality for $B - V$ with SL = 99.5% (more than 2.5 σ). Tests for $B - R$ give a significance level of 97.1% (more than 2 σ). The algorithm applied here is exactly the same as in Peixinho et al. (2003). In our case, there is a stronger result for $B - V$ than for $B - R$. It is also interesting to note the differences in results between the K-S test and the dip test. The latter is specifically designed to detect a bimodal structure and is therefore more robust for this task than the K-S test: its results should be regarded as the most conservative. This indicates that the Centaur $B - V$ and $B - R$ bimodality is not a closed subject yet and deserves a more thorough study (which is far beyond the scope of the present work).

TABLE 9
DIP TEST RESULTS FOR THE CENTAURS

Color	n[a]	Dip	SL (%)
$J - H$	15	0.071	25.0
$H - K$	17	0.070	32.0
$J - K$	15	0.112	91.9
$V - J$	10	0.087	38.3
$B - V$	17	0.136	99.5
$B - R$	17	0.121	97.1

[a] Number of objects in the sample studied.

7. SUMMARY

We used the 8 m Very Large Telescope at Cerro Paranal (Chile) and the ISAAC instrument to perform near-IR *JHK* broadband photometry on a sample of 17 KBOs and Centaurs. We compiled visible–infrared colors (*VJHK*) from both the published literature and this paper for a total of 51 objects. Two outliers, (24835) 1995 SM_{55} and (19308) 1996 TO_{66}, display peculiar near-IR colors. Both objects were reported to have nonrepeatable visible light curves over time. We performed several statistical tests on the sample of 51 visible–infrared colors to study the following:

1. The color-color correlations.
2. The color–physical parameter (i.e., orbital parameters and absolute magnitude) dependences.
3. The structure of Centaur color distributions (e.g., continuous or bimodal).

Centaurs show some 3 σ level color-color correlations that are consistent with the presence of a coloring process that would be acting on surface colors over the visible–near-IR range (0.4–2.5 μm). Results also show that the Centaurs have a quasi-linear reflectivity spectrum over the $V \rightarrow J$ spectral range (as previously reported in McBride et al. 2003; Delsanti et al. 2004). The $H - K$ index (17 objects) correlates with the visible colors and spectral gradient (2.5 σ level): the optically reddest Centaurs show $H - K$ colors that are systematically bluer than the Sun (as illustrated in Fig. 3). The surfaces of these objects with a negative spectral slope in the $H \rightarrow K$ range might harbor some chemical components with spectral signatures around 1.7–2.2 μm (ices such as those for H_2O, CH_4, and NH_3, silicates, or complex organic materials such as Titan tholins). Only a proper near-IR spectroscopic study can unveil the nature of these absorptions. Among the eight objects with $H - K$ colors bluer than the Sun, three have been measured with near-IR spectroscopy. Water ice was detected on their surfaces (evidenced by a broad feature around 2 μm).

Centaurs show no statistically significant bimodal structure in their near-IR (*JHK*) color distributions (samples of 15–17 objects), as tested with the K-S and dip test tools (see Tables 8 and 9). The $B - R$ color distribution of the sample studied shows some statistically significant evidence for a bimodal structure, which is compatible with results from Peixinho et al. (2003) on different data.

Classical objects show no 3 σ level correlations. However, at a lower significance level the results are consistent (as for Centaurs) with a coloring process affecting the surfaces in the visible–near-IR range. The $V - J$ index is correlated with perihelion distance q: objects with a shorter perihelion distance show bluer colors. The same trend was reported by Doressoundiram et al. (2005) for the $B - R$ colors. We consider this result interesting (see Fig. 4, *bottom*) yet marginal (11 objects, a correlation coefficient of 0.67

for a significance level of 97.6%) and would recommend monitoring this trend with a growing color sample.

Resonant and scattered disk objects are underrepresented with respect to classical KBOs or Centaurs. Scattered disk objects (seven objects only) show strictly no results with SL $> 90\%$. Resonant objects show a marginal dependence of $V - J$ on semimajor axis a that should be confirmed with a larger sample.

A. Delsanti thanks C. de Bergh for valuable comments and I. Belskaya for sharing unpublished results. A. Delsanti acknowledges support from the NASA Astrobiology Institute under cooperative agreement NNA04CC08A at the Institute for Astronomy (University of Hawaii, Manoa). N. Peixinho acknowledges funding from the Portuguese Foundation for Science and Technology (FCT-SFRH:BD/1094/2000).

REFERENCES

Barucci, M. A., ed. 2003, New Frontiers in the Solar System: Trans-Neptunian Objects (Comptes Rendus de l'Academie des Sciences 4[7]; Paris: Academie des Sciences)
Barucci, M. A., Doressoundiram, A., & Cruikshank, D. 2004, in Comets II, ed. M. C. Festou, H. U. Keller, & H. A. Weaver (Tucson: Univ. Arizona Press), 647
Barucci, M. A., Doressoundiram, A., Tholen, D., Fulchignoni, M., & Lazzarin, M. 1999a, Icarus, 142, 476
Barucci, M. A., Lazzarin, M., & Tozzi, G. P. 1999b, AJ, 117, 1929
Barucci, M. A., et al. 2002, A&A, 392, 335
Bauer, J., Meech, K., Fernandez, Y., Pittichova, J., Delsanti, A., Boehnhardt, H., & Hainaut, O. R. 2003, Icarus, 166, 195
Belskaya, I. N., Ortiz, J. L., Rousselot, P., Ivanova, V., Borisov, G., Shevchenko, V. G., & Peixinho, N. 2005, in Abstracts from Asteroids, Comets, and Meteors 2005 (Rio de Janeiro: Observatório Nacional), http://www.on.br/acm2005/abstract.html
Boehnhardt, H., et al. 2001, A&A, 378, 653
———. 2002, A&A, 395, 297
Brown, M. E. 2000, AJ, 119, 977
Brown, M. E., & Koresko, C. C. 1998, ApJ, 505, L65
Brown, R. H., Cruikshank, D. P., & Pendleton, Y. 1999, ApJ, 519, L101
Chiang, E. I., et al. 2003, AJ, 126, 430
Cruikshank, D. P., et al. 1998, Icarus, 135, 389
Davies, J. 2000, in Minor Bodies in the Outer Solar System, ed. A. Fitzsimmons, D. Jewitt, & R. M. West (Berlin: Springer), 9
Davies, J. K., & Barrera, L., eds. 2004, The First Decadal Review of the Edgeworth-Kuiper Belt (Earth Moon Planets 92 [2003]; Dordrecht: Kluwer)
Davies, J. K., Green, S., McBride, N., Muzzerall, E., Tholen, D. J., Whiteley, R. J., Foster, M. J., & Hillier, J. K. 2000, Icarus, 146, 253
Davies, J. K., McBride, N., Ellison, S. L., Green, S. F., & Ballantyne, D. R. 1998, Icarus, 134, 213
Davies, J. K., Sykes, M. V., & Cruikshank, D. P. 1993, Icarus, 102, 166
Delsanti, A., Hainaut, O., Jourdeuil, E., Meech, K., Boehnhardt, H., & Barrera, L. 2004, A&A, 417, 1145
Delsanti, A., & Jewitt, D. 2006, in Solar System Update (Berlin: Springer Praxis), in press
Doressoundiram, A., Barucci, M. A., Tozzi, G., Poulet, F., Boehnhardt, H., de Bergh, C., & Peixinho, N. 2006, Planet. Space Sci., in press
Doressoundiram, A., Peixinho, N., de Bergh, C., Fornasier, S., Thébault, P., Barucci, M. A., & Veillet, C. 2002, AJ, 124, 2279
Doressoundiram, A., Peixinho, N., Doucet, C., Mousis, O., Barucci, M. A., Petit, J. M., & Veillet, C. 2005, Icarus, 174, 90
Doressoundiram, A., Tozzi, G. P., Barucci, M. A., Boehnhardt, H., Fornasier, S., & Romon, J. 2003, AJ, 125, 2721
Dotto, E., Barucci, M. A., Boehnhardt, H., Romon, J., Doressoundiram, A., Peixinho, N., de Bergh, C., & Lazzarin, M. 2003, Icarus, 162, 408
Duncan, M. J., Levison, H. F., & Budd, S. M. 1995, AJ, 110, 3073
Efron, B., & Tibshirani, R. 2003, An Introduction to the Bootstrap (Boca Raton: Chapman & Hall/CRC)
Fasano, G., & Franceschini, A. 1987, MNRAS, 225, 155
Fornasier, S., et al. 2004, A&A, 421, 353
Gladman, B., Holman, M., Grav, T., Kavelaars, J., Nicholson, P., Aksnes, K., & Petit, J.-M. 2002, Icarus, 157, 269
Green, S. F., McBride, N., O'Ceallaigh, D. P., Fitzsimmons, A., Williams, I. P., & Irwin, M. J. 1997, MNRAS, 290, 186
Grundy, W. M., Noll, K. S., & Stephens, D. C. 2005, Icarus, 176, 184
Hainaut, O. R., & Delsanti, A. C. 2002, A&A, 389, 641
Hainaut, O. R., et al. 2000, A&A, 356, 1076
Hardorp, J. 1980, A&A, 88, 334
Hartigan, J., & Hartigan, P. 1985, Ann. Stat., 13, 70
Hartmann, W. K., Cruikshank, D. P., & Degewij, J. 1982, Icarus, 52, 377
Hartmann, W. K., Cruikshank, D. P., Degewij, J., & Capps, R. W. 1981, Icarus, 47, 333
Imanaka, H., et al. 2004, Icarus, 168, 344
Jewitt, D., & Luu, J. 1993, Nature, 362, 730
———. 1998, AJ, 115, 1667
Khare, B. N., Sagan, C., Arakawa, E. T., Suits, F., Callcott, T. A., & Williams, M. W. 1984, Icarus, 60, 127
Kolmogorov, A. 1933, Giornale deli Instituto Italiano degli Attuari, 4, 83
Lazzarin, M., Barucci, M. A., Boehnhardt, H., Tozzi, G. P., de Bergh, C., & Dotto, E. 2003, AJ, 125, 1554
Luu, J., & Jewitt, D. 1996, AJ, 112, 2310
McBride, N., Davies, J., Green, S., & Foster, M. 1999, MNRAS, 306, 799
McBride, N., Green, S. F., Davies, J. K., Tholen, D. J., Sheppard, S. S., Whiteley, R. J., & Hillier, J. K. 2003, Icarus, 161, 501
Peacock, J. 1983, MNRAS, 202, 615
Peixinho, N., Boehnhardt, H., Belskaya, I., Doressoundiram, A., Barucci, M., & Delsanti, A. 2004, Icarus, 170, 153
Peixinho, N., Doressoundiram, A., Delsanti, A., Boehnhardt, H., Barucci, M., & Belskaya, I. 2003, A&A, 410, L29
Persson, S. E., Murphy, D. C., Krzeminski, W., Roth, M., & Rieke, M. J. 1998, AJ, 116, 2475
Romon-Martin, J., Barucci, M. A., de Bergh, C., Doressoundiram, A., Peixinho, N., & Poulet, F. 2002, Icarus, 160, 59
Sagan, C., Khare, B. N., Thompson, W. R., Murray, B. G. J. P. T., & Squyres, S. W. 1984, BAAS, 16, 668
Sekiguchi, T., Boehnhardt, H., Hainaut, O. R., & Delahodde, C. E. 2002, A&A, 385, 281
Sheppard, S. S., & Jewitt, D. C. 2003, Earth Moon Planets, 92, 207
Spearman, C. 1904, Am. J. Psychology, 52, 72
Tegler, S., & Romanishin, W. 1998, Nature, 392, 49
———. 2000, Nature, 407, 979
———. 2003, Icarus, 161, 181
Trujillo, C. A., & Brown, M. E. 2002, ApJ, 566, L125
Weintraub, D. A., Tegler, S. C., & Romanishin, W. 1997, Icarus, 128, 456